Efficient Probabilistic Prediction and Uncertainty Quantification of Hurricane Surge and Inundation

William J. Pringle,[a] Zachary Burnett,[b,c] Khachik Sargsyan,[d] Saeed Moghimi,[b] Edward Myers,[b]

[a] *Environmental Science Division, Argonne National Laboratory, Lemont, IL, USA*

[b] *Coast Survey Development Laboratory, National Oceanic and Atmospheric Administration (NOAA), Silver Spring, MD, USA*

[c] *University Corporation for Atmospheric Research (UCAR), Boulder, CO, USA*

[d] *Sandia National Laboratories, Livermore, CA, USA*

Corresponding author: William J. Pringle, wpringle@anl.gov

ABSTRACT: This study proposes a methodology for efficient probabilistic prediction of near-landfall hurricane-driven storm surge, tide, and inundation. We perturb forecasts of hurricane track, intensity, and size according to quasi-random low-discrepancy Korobov sequences of historical forecast errors with assumed Gaussian and uniform statistical distributions. These perturbations are run in an ensemble of hydrodynamic storm tide model simulations, and the resulting set of maximum water surface elevations are used as a training set to develop a Polynomial Chaos (PC) surrogate model from which global sensitivities and probabilistic predictions can be extracted. The maximum water surface elevation is extrapolated over dry points incorporating energy head loss with distance to properly train the surrogate for predicting inundation. We find that the surrogate constructed with 3rd order PCs using Elastic Net penalized regression with Leave-One-Out cross-validation provides the most robust fit across training and validation sets. Probabilistic predictions of maximum water surface elevation and inundation area by the surrogate at 48-hour lead time for three past U.S. landfalling hurricanes (Irma 2017, Florence 2018, and Laura 2020) are found to be reliable when compared to best-track hindcast simulation results, even when trained with as few as 19 samples. The maximum water surface elevation is most sensitive to perpendicular track-offset errors for all three storms. Laura is also highly sensitive to storm size and has the least reliable prediction. This methodology is built into an open-source Python framework available from `https://github.com/noaa-ocs-modeling/EnsemblePerturbation`.

SIGNIFICANCE STATEMENT: This purpose of this study is develop and evaluate a methodology that can be used to provide high-quality probabilistic predictions of hurricane-induced storm surge and inundation with limited time and resources. This is important for emergency management purposes during or after the landfall of hurricanes. Our results show that sampling forecast errors using quasi-random sequences combined with machine learning techniques that fit polynomial functions to the data are well-suited to this task. The polynomial functions also have the benefit of producing exact sensitivity indices of storm surge and inundation to the forecasted hurricane properties such as path, intensity, and size, which can be used for uncertainty estimation. The code implementing the presented methodology is publicly available on Github.

1. Introduction

Tropical and subtropical storms build up storm surges that affect populated coastal regions in the U.S. and internationally. The temporarily-higher sea levels from these storm surges result in widespread inundation of coastal low-lying areas, invoking flood and wave damage to residential and commercial structures. Storm surges from named storm events are estimated to cause billions of dollars in damages in the U.S. annually (NOAA National Centers for Environmental Information (NCEI) 2022). Under the requirements of the part of the Consumer Option for an Alternative System to Allocate Losses (COASTAL) Act, the National Oceanic and Atmospheric Administration (NOAA) is responsible for determining the extent of storm surge and storm tide to inform response and application of relief funding from the Federal Emergency Management Administration (FEMA) after a storm event.

While currently not in operation, in this project we are investigating the application of a Hurricane Surge On-demand Forecast System (HSOFS) that could be employed when a tropical cyclone (TC) approaches and makes landfall along U.S. coastlines to provide predictions of hurricane-driven storm surge and inundation (Vinogradov et al. 2018). HSOFS uses a hydrodynamic storm tide model to simulate coastal water levels and inundation on high-resolution unstructured meshes, which may also be coupled to a wind-wave model to capture wave setup effects (Dietrich et al. 2011; Moghimi et al. 2020). The system would be utilized to produce either; 1) near-landfall forecasts for support of recovery and response in the immediate aftermath of hurricane landfall, or 2) hindcasts for allocating flooding-related insurance losses as part of the COASTAL Act (Abdolali et al. 2021). But as with any modeling, the uncertainty in the results are dependent on the uncertainty and accuracy of the input parameters, predominantly those of the hurricane track, intensity, and size. Therefore, it is becoming increasingly important to provide probabilistic predictions and uncertainty estimates for decision making. Obtaining the probabilistic result makes the predictions more informative and robust, and reduces the likelihood of overestimation or underestimation of the severity of storm surge.

However, the complexity of HSOFS, which was previously in operation, leads to a relatively high computational load, limiting the number of model ensembles achievable in a time and resource-limited environment. This has been an obstacle in the development of a probabilistic version. In contrast, the National Hurricane Center's (NHC) Probabilistic Tropical Storm Surge (P-Surge) model (Taylor and Glahn 2008) performs hundreds of ensemble simulations within the allotted one hour time-frame (~30 min per simulation per CPU) through an ad-hoc full factorial perturbation of estimated hurricane track, intensity and size errors. P-Surge is based on the Sea, Lake, and Overland Surges from Hurricanes (SLOSH) hydrodynamic code (Jelesnianski et al. 1992), which makes several physical simplifications (Joyce et al. 2019) and employs limited-area meshes for efficiency. Thus, the aim of this study is to develop an efficient ensemble prediction framework (requiring few model simulations) that can be used by the more comprehensive and computationally intensive HSOFS model for accurate near-landfall probabilistic forecasts of hurricane surge and inundation.

To this end, Davis et al. (2010) divided the range of the hurricane track errors into equal-area bins depending on a user-defined priority level, and estimated that 27 ensemble members resolved 90% of inundation. Additionally, Kyprioti et al. (2021a) showed that quasi-Monte Carlo methodologies can be used to improve sampling efficiency of hurricane parameter errors over the full factorial approach used by P-Surge. However, there may still be limitations in the information available from smaller model ensembles [$O(10)$] that we aim for here. A possible solution is to seek a surrogate approximation that can be used to rapidly sample a wider distribution of input hurricane parameters and obtain robust statistical quantities, without having to query and iterate over the costly hydrodynamic model.

Many such surrogate models for storm surge prediction have been proposed, using machine learning techniques such as Gaussian Processes (GP; kriging), artificial neural networks (ANN), and convolution neural networks (CNN), often combined with dimensionality reduction and k-means clustering via Principal Component Analysis (PCA) (e.g., Jia and Taflanidis 2013; Taflanidis et al. 2013; Kim et al. 2015; Hashemi et al. 2016; Lee et al. 2021; Kyprioti et al. 2021b; Plumlee et al. 2021). This approach often involves training a surrogate model using a large ensemble of synthetic hurricanes which can then be used to predict the storm surge based on the current hurricane parameters as inputs (Taflanidis et al. 2013; Kim et al. 2015; Hashemi et al. 2016; Lee et al. 2021). As noted by Lee et al. (2021), one of the limitations of this approach is that nonlinear interactions of surge with other processes (e.g., astronomical tides, background sea levels, and rainfall) are ignored, which could be particularly important for inundation behavior. A potential solution is to generate a new surrogate model for the current storm that includes (some of) these interactions in the hydrodynamic model, as most recently explored by Plumlee et al. (2021) using GPs.

In this study we also seek a solution that develops a surrogate model on-the-fly to provide both robust statistics and uncertainty information of storm surge and flooding predictions for the current storm. A method potentially well-suited to this application is Polynomial Chaos (PC) theory, which has been recently used for developing probabilistic predictions and analyzing the sensitivity of surge to hurricane parameters with good success (Sochala et al. 2020; Ayyad et al. 2021). PC is a convenient means to propagate uncertainties from inputs to outputs of interest for general computational models (Sargsyan 2017). It can further be interrogated to rapidly evaluate moments and sensitivities due to their analytical availability, or quantiles and probability density functions (PDFs) via computationally inexpensive sampling. Thus, in this study we adopt PC theory and develop strategies around efficient random variable sampling, dimensionality reduction, penalized regression with cross-validation, and manipulation of the training set to optimize the setup for PC construction. We evaluate the accuracy of this PC-based surrogate model and demonstrate the reliability of the probabilistic prediction for three historical U.S. landfalling hurricanes (Irma 2017, Florence 2018, and Laura 2020). Statistical quantities and variance-based sensitivities from the PC surrogate can be distributed along with surrogate itself as a product of the ensemble HSOFS modeling system. The ensemble generation and PC analysis methodology presented in this paper is implemented in an open-source Python framework called `EnsemblePerturbation`.

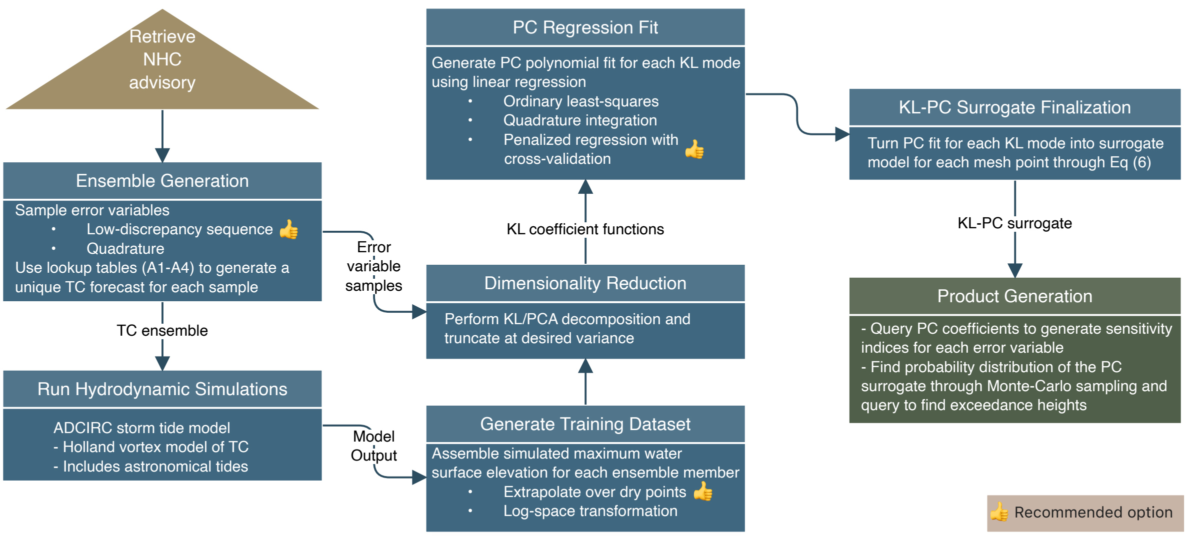

FIG. 1. Flowchart of the proposed methodology for efficient probabilistic predictions and uncertainty quantification of hurricane storm surge and inundation.

2. Methods and Experiment

A flowchart of the proposed methodology in this study is shown in Fig. 1. To fully comprehend components of the flowchart we refer the reader to the rest of this section (a-d), as well as to the results section 3 for details. Finally, in section e we describe the experiments we conduct to assess the accuracy of different options and evaluate the reliability of the probabilistic prediction.

a. Storm Surge Modeling Component of the On-demand System

The hydrodynamic storm tide model is based on the ADvanced CIRCulation (ADCIRC; Luettich and Westerink 2004) code, which solves the shallow water equations using the continuous Galerkin finite-element method over an unstructured triangular mesh. ADCIRC is also the modeling engine for the Global Surge and Tide Operational Forecast System (`https://registry.opendata.aws/noaa-gestofs/`). In this study we use version 55 of ADCIRC (Pringle et al. 2021) including both astronomical tides and atmospheric-driven surge, but without coupling to a wind-wave model to capture the wave setup effect. Parametric representations of the TC vortex (based on track advisories provided by the NHC) are used to construct surface wind and pressure forcing driving storm surge in the ADCIRC model. Here, we use the classical symmetrical Holland vortex model

(Holland 1980) that is built directly into the ADCIRC code. The unstructured mesh used in this study encompasses the western North Atlantic and Gulf Coast region with 1.81 million vertices, and resolution ranges from roughly 200 m at the coast and overland up to a maximum of 46 km in the open ocean (Technology Riverside Inc. and AECOM 2015). The vertical datum is mean sea level (MSL) and the floodplain extends up to an elevation of 10 m above MSL. Manning's n friction coefficients, surface canopy coefficients, and surface directional effective roughness lengths based on land use data are used to account for surface roughness effects on the hydrodynamics and to modify the atmospheric forcing overland, respectively (Technology Riverside Inc. and AECOM 2015).

b. Tropical Cyclone Perturbation

In this study, the forecasted TC is perturbed according to historical NHC forecast error statistics of position, intensity, and size (Taylor and Glahn 2008). Positional members are perturbed based on estimated errors for cross-track (CT) and along-track (AT), whereby CT refers to a perpendicular offset of the forecast track and AT refers to a slowdown or speedup of the TC along the forecasted track. Intensity is described by both maximum sustained wind speed (V_{max}) and minimum central pressure (P_c), which is related through the B parameter of the Holland model (Holland 1980), $V_{max}^2 = B(P_b - P_c)/(e\rho)$, where e is the base of natural logarithms, ρ is the air density, and P_b is the background air pressure. We choose V_{max} as the independent perturbed variable and P_c becomes a dependent variable based on keeping the B parameter consistent with the original forecast. The size of the TC is changed by perturbing the radius to maximum winds (R_{max}).

Perturbation of CT, AT, and V_{max} across the whole forecast is achieved through a look-up table of historical NHC mean absolute forecast errors for certain lead times, distributed with the P-Surge model (Penny and Cangialosi 2019) and included here in Tables A1-A3. TCs are divided into three intensity bins based on the initial 0-hr V_{max} due to different error statistics between these categories. For instance, the mean absolute CT error is 11.6 nm at the 12-hr lead time and 27.8 nm at the 48-hr lead time for the medium strength TC (50-95 kt). In this way if we perturb the CT variable by one 'mean absolute error' the track will be offset a perpendicular distance from the original position of 11.6 nm at the 12-hr mark and 27.8 nm at the 48-hr mark. The same idea is true for AT and V_{max}. The CT, AT and V_{max} errors are treated as Gaussian random variables

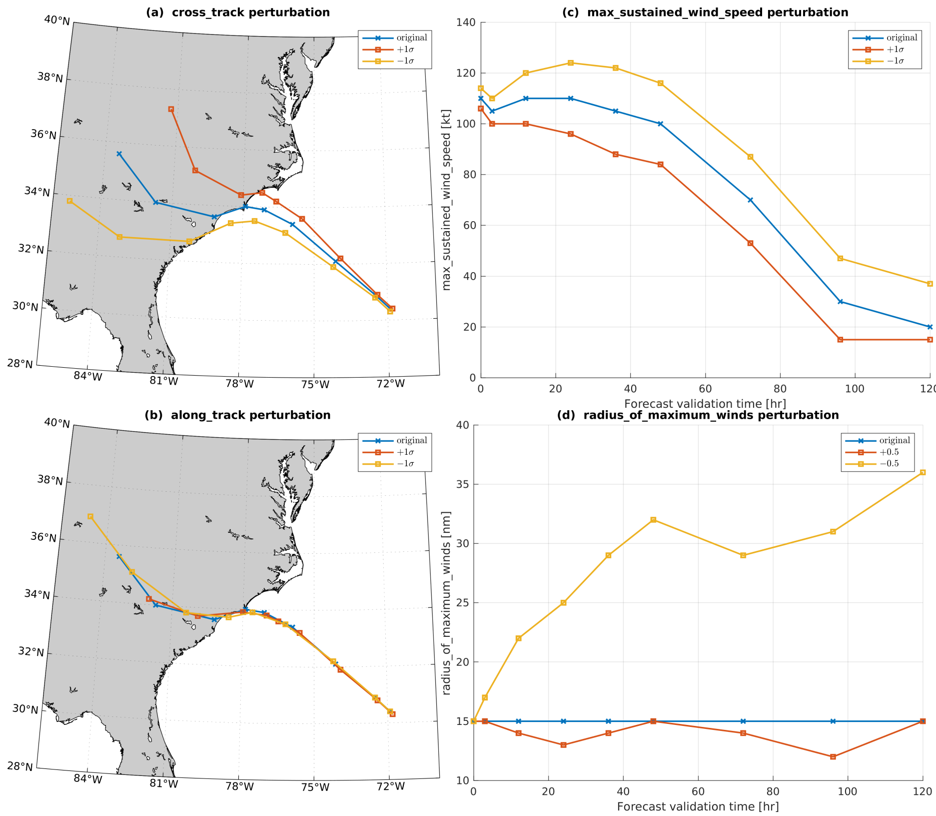

FIG. 2. Example perturbations of a NHC hurricane advisory (Hurricane Florence) along the forecast. $\pm 1\sigma$ perturbations for the Gaussian distributed (a) CT, (b) AT, and (c) V_{max} errors, and ± 0.5 value perturbation of the uniformly distributed (d) R_{max} errors.

($\mu = 0$, $\sigma = 1$) whereby the mean absolute error is defined as 0.7979σ (Gonzalez and Taylor 2018). A negative value will perturb the CT and AT in one direction and positive value in the other, and similarly for V_{max} a negative value corresponds to an intensity underestimate of the forecast and vice-versa for a positive value (see Fig. 2 for an illustration of $\pm 1\sigma$ perturbations). Note that we enforce [15,175] kt bounds on V_{max}.

For R_{max} the idea is similar to the other variables except that at each lead time the perturbation is only from the initialized 0-hr value as NHC does not provide estimates of R_{max} along the forecast. Unlike the other variables, the R_{max} error is bounded and treated as a random variable with a uniform distribution ($\in$[-1,1]) where the upper and lower error bounds at each lead time are found through a look-up table with the TCs divided into five size bins based on the initialized 0-hr R_{max} (Table A4). We determined these upper and lower error bounds by linearly extrapolating the values used by P-Surge at the 15th, 50th and 85th percentile to the 0th and 100th percentile. Referring to Table A4, an initially small storm is skewed towards having negative R_{max} forecast errors (becoming larger along the forecast), and vice-versa for initially large storms (see Fig. 2 for an illustration of ±0.5 perturbations). Note that we enforce [5,200] nm bounds on R_{max}.

c. Ensemble Generation

An ensemble of TC forecasts is generated by sampling the random variables (CT, AT, V_{max} and R_{max} errors) based on the probabilistic property of each variable equally, for forward uncertainty propagation analysis (section d). The idea is to build a surrogate model based on relatively few samples [$O(10)$], which can be then trivially queried to generate the probabilistic forecast, as well as conduct a global sensitivity analysis or obtain a forecast given user-defined values of the TC error variables. In contrast, P-Surge employs an ad-hoc full factorial sampling methodology whereby 7 perturbations of AT (slow to fast) and 3 of V_{max} and R_{max} (weak/large, "medium", and strong/small) are used, along with enough perturbations of CT to cover 90% of the Gaussian distribution with spacing R_{max} at the 48-hr forecast (Gonzalez and Taylor 2018). Each possible permutation is used where each TC event is assigned a weight based on the combined probability and the probabilistic result is determined through summation of the weighted model results. This leads to 63 TC events per CT perturbation, or ~400-900 TC events based on 7 to 15 CT perturbations (Kyprioti et al. 2021a), which would be prohibitive for HSOFS in a resource and time-limited environment.

We sample the variables using a quasi-random low-discrepancy sequence, of which several are available in the `chaospy` python package (Feinberg and Langtangen 2015) employed by `EnsemblePerturbation`, including widely-used Sobol and Halton types. Here, we recommend the use of the Korobov sequence (Korobov 1959) because the random variables are sampled symmetrically about zero and cover a predictable range across all variables for any given sample size, which is not the case for the other `chaospy` sequence implementations. The benefit of such low-discrepancy sequences is avoidance of the "curse of dimensionality" that is associated with quadrature integration, which the P-Surge methodology could be viewed as a subset of. For instance, 3rd order quadrature integration for the four-dimensional problem requires $4^4 = 256$ samples, as all possible permutations of just four perturbations of each variable is used. Smolyak sparse grid quadrature can be used to alleviate the issue, although ~150 samples are still required

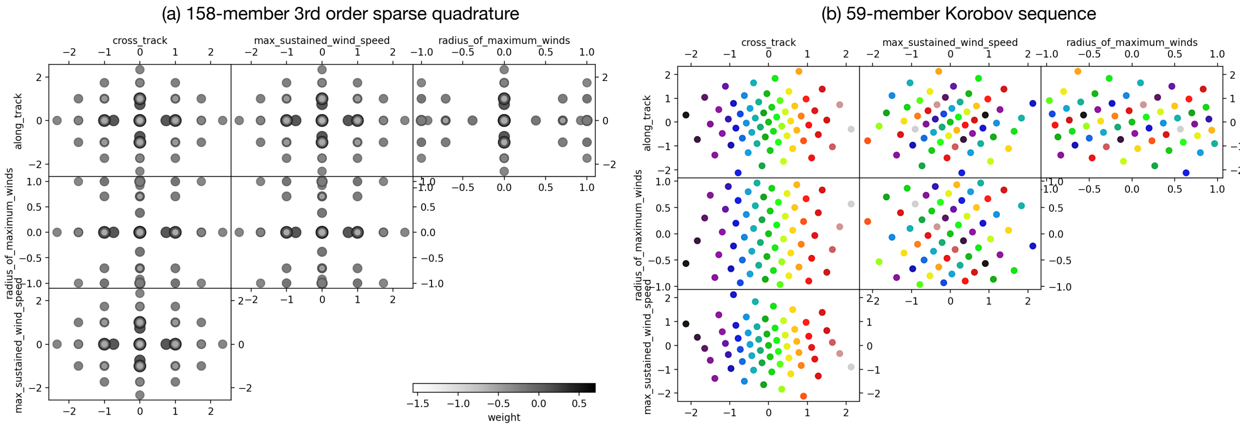

FIG. 3. Perturbed values of λ across the four dimensional space for (a) sparse quadrature and (b) Korobov sequence sampling methodologies. Sparse quadrature has variable weights attached to each perturbation sample (indicated by marker gray-scale and size) while the Korobov sequence is equally weighted (marker colors are used to distinguish unique samples across the panels).

for 3rd order quadrature. Instead, a low-discrepancy sequence can be used to sample each variable more densely without imposing the condition of using all permutations across the four-dimensional space, as illustrated in Fig. 3. Later we show that these low-discrepancy sequences with sample size $O(10)$ can be used to generate a surrogate model that, due to enhanced regression techniques, are indeed of improved quality over the sparse quadrature.

d. Forward Uncertainty Propagation

We wish to know a probabilistic form of the model output $Z = f(\boldsymbol{\lambda}, \boldsymbol{x})$ (maximum water surface elevation in $\boldsymbol{x}$) which is dependent on the set of input TC error parameters, $\boldsymbol{\lambda}$ = (CT, AT, V_{max}, R_{max}). However, the underlying hydrodynamic storm tide model is too computationally expensive to sample a large number of times to properly understand the uncertainty and sensitivity of Z to the TC error variables. Therefore, we employ a surrogate approximation $g(\boldsymbol{\lambda}, \boldsymbol{x}) \approx f(\boldsymbol{\lambda}, \boldsymbol{x})$ through PC theory (Sargsyan 2017; Sochala et al. 2020), which is constructed from a training set (section c). The resulting PC surrogate model is then a parametric representation of Z which can be trivially sampled a large number of times, and from which moments and global sensitivities can be analytically extracted. To ensure a suitable training set for generating an accurate PC surrogate

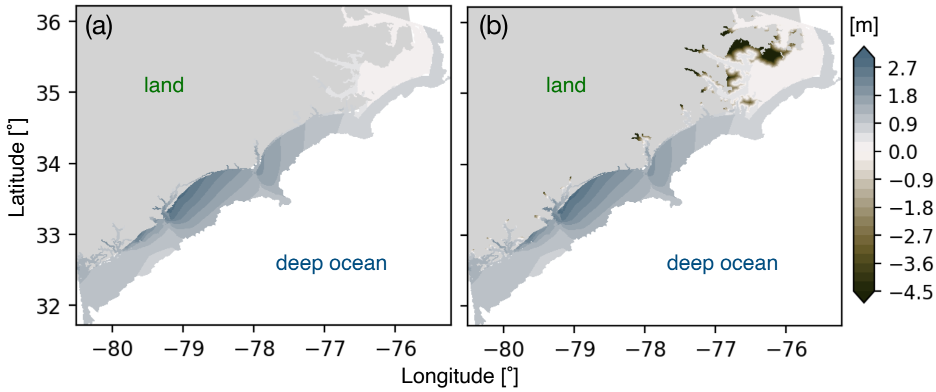

Fig. 4. Example of maximum water surface elevation extrapolation over dry mesh points for a Hurricane Florence training set member. (a) water surface elevations before extrapolation, (b) water surface elevations after extrapolation. Note that mesh points with ocean depths greater than 25 m have been removed from the dataset.

(which requires a degree of smoothness) we manipulate Z and apply a dimensionality reduction technique for computational efficiency. These methodologies are outlined in the rest of this section.

1) Model Output Manipulation

There are two related difficulties that we encounter here with using the maximum water surface elevation for training the PC surrogate: 1) Some mesh points are inundated during some TC events and not in others, and; 2) water surface elevation cannot physically go below the ground elevation (water depth must be positive or zero) but the surrogate model cannot be easily constrained to prevent a physically unrealistic negative depth prediction.

In the first problem the intuitive solution is to set Z to that of the ground elevation for mesh points that are not inundated (denoted 'NaN') in a certain TC event. However, this does not distinguish between TC events where the mesh point of concern might be have been close to being inundated or very far from being inundated, resulting in a poor PC fit for predicting inundation. The solution we propose is to artificially extrapolate Z from wet mesh points over dry mesh points for the PC surrogate training purposes (Fig. 4). Here, we use an inverse-distance weighting (IDW) extrapolation (Plumlee et al. 2021) with a hydraulic head loss factor,

$$\tilde{Z}_d = \frac{\sum_{w=1}^{k} (Z_{dw} - h_{dw}) D_{dw}^{-p}}{\sum_{w=1}^{k} D_{dw}^{-p}} \tag{1}$$

where $\tilde{Z}_d$ is the artificial maximum water surface elevation of the dry mesh point d, Z_{dw} is the maximum water surface elevation of the w^{th} closest wet mesh point to d, D_{dw} is the distance from mesh point w to d, p is the IDW extrapolation order, k is the number of nearest neighbors to use for extrapolation, and h_{dw} is the head loss (Rucker et al. 2021) from mesh point w to d,

$$h_{dw} = D_{dw} f_f \tag{2}$$

where f_f is a hydraulic friction factor. This methodology is similar to the weighted k nearest neighbour pseudo-surge methodology used by Kyprioti et al. (2021c), in which there are four free parameters of the weighting scheme that require calibration. Ostensibly, the head loss factor we use here adds some physical meaning to the extrapolation. The factor f_f can be related to Manning's equation like in Rucker et al. (2021), requiring the Manning's n friction coefficient, flow velocity, and flow depth. These flow quantities are not available once Z is extrapolated over the dry regions so we simply view this relation in terms of guiding f_f to a physically reasonable value. In section 2 we compare values for f_f, k, and p and how they affect surrogate model prediction accuracy.

A possible solution to the second problem is to build the surrogate model based on $\log(H)$ (Plumlee et al. 2021), where H is the simulated maximum water depth, which is physically always positive, guaranteeing that the surrogate prediction will be positive. However, an issue we find here is that our water surface elevation extrapolation technique proposed above leads to artificial negative water depths for otherwise dry mesh points in the training set. Therefore, H in the training data would need to modified to be positive for these points by adding a constant, which can be subtracted back from the surrogate prediction. Of course, this means that the surrogate model can actually predict a negative real water depth for such dry mesh points, just as was provided to it for training. We test the accuracy of constructing the surrogate in log-space versus linear-space in section 2.

2) Dimensionality Reduction and Polynomial Chaos Surrogate

Building a surrogate model for all HSOFS mesh points (1.81 million), or even a subset of points around hurricane landfall [$O(10^5)$], would be prohibitively expensive, therefore we seek a method to reduce the dimensionality of the problem. Such dimensionality reduction is common practice and has been used for building other surge surrogate models (e.g., Jia et al. 2016; Sochala et al.

2020; Kyprioti et al. 2021b; Lee et al. 2021). Here, we achieve dimensionality reduction via Karhunen-Loève (KL) expansions which are then coupled with PC surrogates.

As before, our model output of maximum water surface elevations, $Z = f(\boldsymbol{\lambda}, \boldsymbol{x})$ is dependent on the set of input TC error parameters, $\boldsymbol{\lambda}$ and is spatially varying with $\boldsymbol{x}$. The KL expansion can be written as,

$$Z = f(\boldsymbol{\lambda}, \boldsymbol{x}) = \bar{f}(\boldsymbol{x}) + \sum_{j=1}^{L} \xi_j(\boldsymbol{\lambda})\sqrt{\mu_j}\phi_j(\boldsymbol{x}) \tag{3}$$

in terms of uncorrelated, zero-mean, unit-variance random variables $\xi_j(\boldsymbol{\lambda})$ and eigenvalue-eigenfunction pairs $(\mu_j, \phi_j(\boldsymbol{x}))$ of the covariance,

$$C(\boldsymbol{x}, \boldsymbol{x}') = E_{\boldsymbol{\lambda}}[(f(\boldsymbol{\lambda}, \boldsymbol{x}) - \bar{f}(\boldsymbol{x}))(f(\boldsymbol{\lambda}, \boldsymbol{x}') - \bar{f}(\boldsymbol{x}'))] \tag{4}$$

truncated at eigenvalue $L(\ll$ dimensions of $\boldsymbol{x})$ that explains a user-defined level of variance. The expectation $E_{\boldsymbol{\lambda}}$ indicates averaging across parameter $\boldsymbol{\lambda}$, as does the bar symbol, i.e., $\bar{f}(\boldsymbol{x}) = E_{\boldsymbol{\lambda}}[f(\boldsymbol{\lambda}, \boldsymbol{x})]$. The forward uncertainty propagation problem therefore reduces to seeking a function approximation for the KL coefficient functions $\xi_j(\boldsymbol{\lambda})$, for which we employ a PC form here,

$$\xi_j(\boldsymbol{\lambda}) \approx \sum_{k=0}^{K} c_{jk}\Psi_k(\boldsymbol{\xi}) \tag{5}$$

where $\Psi_k(\boldsymbol{\xi})$ are multivariate orthogonal polynomials with respect to the PDF of the stochastic germ $\boldsymbol{\xi}$, which is a vector with elements being standard random variables that are chosen according to the expected PDF of the corresponding element of $\boldsymbol{\lambda}$, i.e., Gauss-Hermite for CT, AT and V_{max} errors and the Legendre-Uniform for R_{max} errors in this study. Finally, by substituting the PC equations (5) into the KL expansion (3) and switching the summations we arrive at the following joint KL-PC surrogate expansion,

$$Z = f(\boldsymbol{\lambda}, \boldsymbol{x}) \approx g(\boldsymbol{\lambda}, \boldsymbol{x}) = \sum_{k=0}^{K} c_k(\boldsymbol{x})\Psi_k(\boldsymbol{\xi}), \qquad \text{where} \tag{6}$$

$$c_k(\boldsymbol{x}) = \delta_{k0}\bar{f}(\boldsymbol{x}) + \sum_{j=1}^{L} c_{jk}\sqrt{\mu_j}\phi_j(\boldsymbol{x}) \tag{7}$$

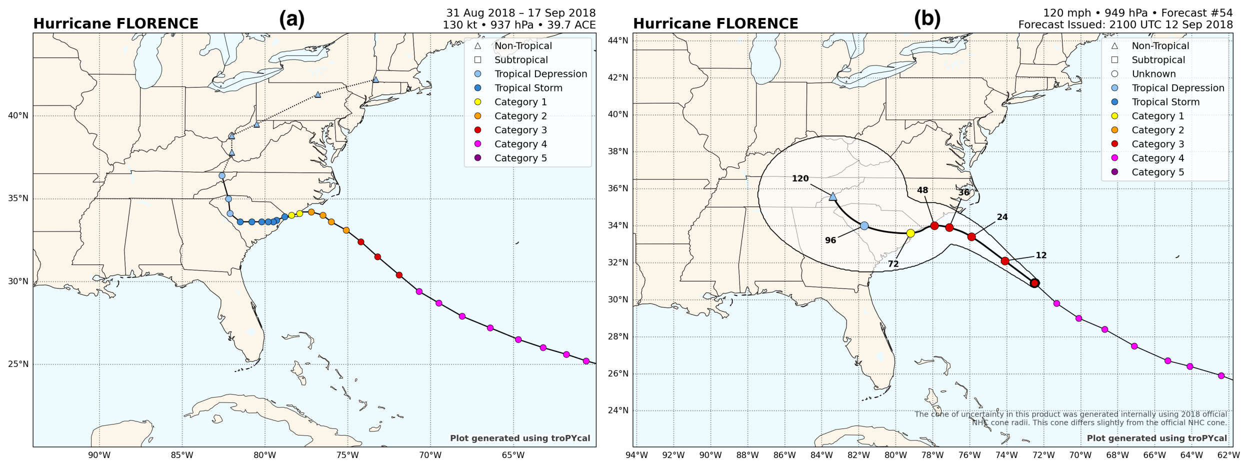

FIG. 5. Hurricane Florence 2018 track and intensity information; (a) best-track hindcast, (b) NHC forecast advisory 48-hr prior to landfall.

and δ is the Kronecker delta. Given the PC coefficients $c_k(\boldsymbol{x})$, moments and global sensitivity indices can be analytically extracted from the KL-PC surrogate expansion (Sargsyan 2017; Sargsyan et al. 2021).

In our python implementation of the joint KL-PC surrogate expansion in `EnsemblePerturbation`, the `scikit-learn` Principal Component Analysis (PCA) class is used to perform the KL decomposition, and the `chaospy` (Feinberg and Langtangen 2015) package is used to perform the PC expansion, utilizing linear regression models from `scikit-learn`. These regression models are introduced and assessed in section 3.

e. Experimental Design

HSOFS is primarily concerned with forecasts of hurricane surge and inundation near (<48-hr) landfall. To provide a rigorous test of the methodologies (section a), in this study we explore results for the 48-hr lead time NHC advisory for three historical US hurricanes; Irma 2017, Florence 2018, and Laura 2020 (e.g., Fig. 5b). The storm tide model is spun-up from a quiescent state with astronomical tides and best-track hindcast forcing (e.g., Fig 5a) for 7-days prior to the forecast. For each hurricane we analyze a subset of the model based on mesh points that have ocean depths $\leq$25 m and that fall within the 34-kt wind speed swath of the NHC advisory. The spatial dimension of this subset is reduced through KL decomposition with truncation at the 99.99% variance level.

In the first set of methodology experiments (section a1) we compare regression models, sampling methods, and sample size for construction of the surrogate model. In these experiments we conduct the analysis in linear-space only on mesh points that are inundated across all TC events to avoid complicating the experiment with the water surface elevation extrapolation over dry mesh points. First, we compare sparse quadrature integration (158 samples) to a 59-member Korobov sequence using different `scikit-learn` regression models for constructing the surrogate model. Then using the best regression model from that experiment we compare Korobov sequences with sample sizes of 19, 39, and 59 which cover 90.0%, 95.0% and 96.7% of the distributions of $\boldsymbol{\lambda}$, respectively. In the second set of methodology experiments (section a2) we conduct the analysis on all mesh points in the subset, in both log-space versus linear-space, and with varying parameters of the water surface elevation extrapolation method. Note that in all cases we use 3rd order PCs which we found to be the only reliable PC order; 2nd order PCs are not flexible enough while the desired size of the training set is too small to allow for higher-order four-dimensional PCs to be constructed accurately.

To validate the surrogate model we use a 128-member validation set for each storm where $\boldsymbol{\lambda}$ is randomly chosen from their distributions for each validation member. To evaluate the accuracy of the surrogate model we compute the root-mean-square-error (RMSE) across the mesh points between the model simulation and the surrogate model for a single validation member. To compare the surrogate model across all validation members we plot cumulative distribution functions (CDFs) of the RMSE and compute the two-sided t-test statistic of the RMSE distribution between two surrogate models. In the second set of experiments we also compute the percentage of mesh points that are falsely classified as wet or dry in the surrogate model prediction.

Finally, using the recommend methodology based on the experiments we construct joint KL-PC surrogate models for each hurricane to produce example products of an ensemble HSOFS, i.e., global sensitivities of Z with respect to $\boldsymbol{\lambda}$, and exceedance probability maps (section b). The probabilistic predictions are compared to simulated model results of the best-track hindcast hurricane forcing. The reliability of the probabilistic prediction is assessed by comparing the fraction of elevation exceedances in the best-track results above the height of the given exceedance probability. Here, mesh points where the predicted exceedance elevation is NaN (dry) are ignored in the computation, while a NaN in the best-track simulation is set to ground elevation. In addition,

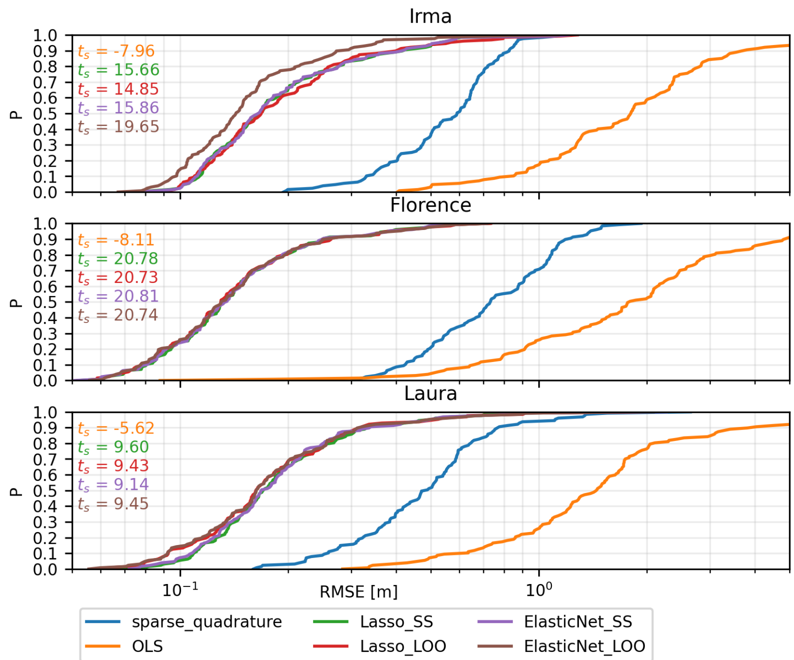

FIG. 6. CDF curves of the surrogate model RMSE across all validation members (128 samples) for the three hurricane forecasts (Irma, Florence, Laura), using a 158-member sparse quadrature training set and a 59-member Korobov sequence training set with different regression methodologies. t_s is the two-sided t-test statistic between the sparse quadrature RMSE and the Korobov RMSEs corresponding to the colors in the legend (largest positive value indicates smallest average RMSE).

inundation area is compared, where we expect the median (50% exceedance probability) prediction to be similar to that of the best-track.

3. Results

a. Methodology Experiments

1) REGRESSION

Results across all three storms show that fitting the surrogate model using (sparse) quadrature integration is superior to Ordinary Least Squares (OLS) linear regression but far inferior to penalized linear regression from the 59-member Korobov sequence (Fig. 6). For this test we compare Lasso and Elastic Net regression that uses ℓ_1-norm regularization and combined ℓ_1-norm and ℓ_2-norm regularization with equal weighting, respectively. ℓ_1-norm regularization penalizes non-zero coef-

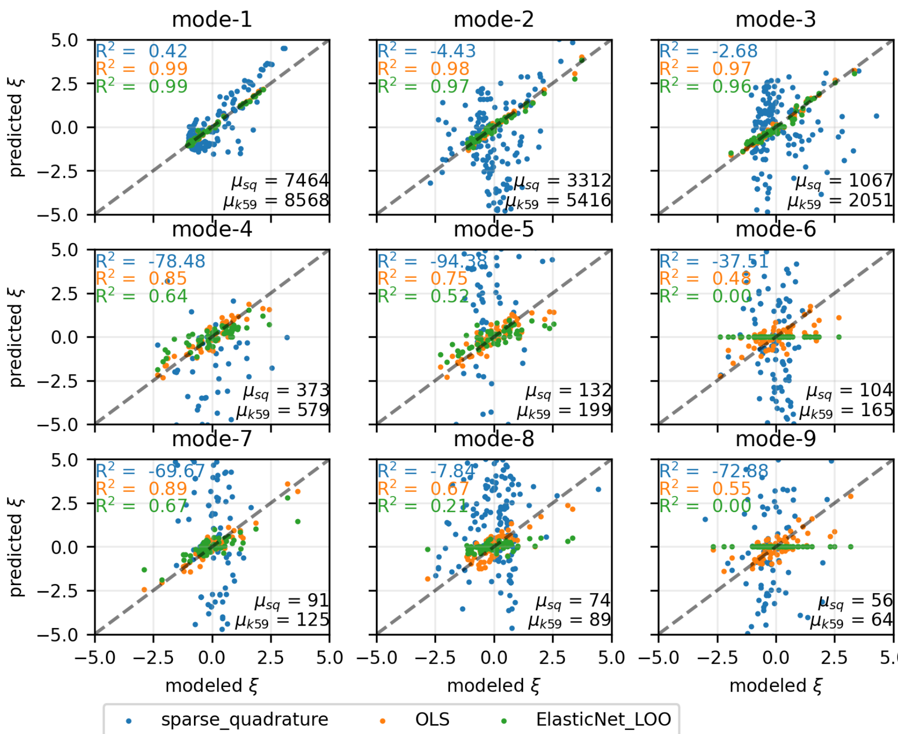

FIG. 7. Comparison of the predicted (surrogate) and modeled KL training parameters, ξ, of the top nine KL modes for the Hurricane Florence forecast. R^2 is the coefficient of determination of the surrogate prediction corresponding to the colors in the legend. μ indicates the eigenvalues of each KL mode evaluated from the sparse quadrature (sq) and 59-member Korobov sequence (k59) training data.

ficients to form sparse models, and ℓ_2-norm regularization penalizes the size of the coefficients to form smooth models. These linear regression models avoid overfitting the KL parameters, ξ, in the training set which we see for OLS regression (Fig. 7), resulting in poor validation. As a rule, the penalized regression gives a poorer fit to the KL training parameters than for the OLS regression, although correlation is generally higher for lower modes. On the other hand, sparse quadrature gives a very poor fit to the KL training parameters, which indeed leads to poor validation relative to the penalized regression. Sparse quadrature projection is known to perform poorly for noisy data due to the presence of negative quadrature weights and amplification of small errors during PC construction (Sargsyan 2012). Nevertheless, sparse quadrature does validate better than OLS regression.

With both Lasso and Elastic Net we use built-in cross-validation estimators to automatically select the best penalization weight and return the most robust fit to the data. Shuffle-Split (SS) and Leave-One-Out (LOO) cross-validation estimators are used to automatically divide up the overall 59-member training set into training and validation subsets during the regression fitting process. Results show that overall there are relatively small differences between the four combinations of cross-validators and regularization strategies, although ElasticNet_LOO notably outperforms for Irma, as well as having a strong performance for both Florence and Laura. Therefore, we decide to use ElasticNet_LOO for the remainder of this paper, remarking also that LOO is attractive because there are no parameter choices to be made, while SS requires choosing the relative size of the training and validation subsets (we used the `scikit-learn` default options here), in which the optimal choice may differ with sample sizes and storms. Furthermore, for Elastic Net regression we can also use cross-validation to select the optimal weighting between ℓ_1 and ℓ_2 penalties if so desired, although we used 0.5 (equal weighting) here for simplicity.

When reducing the training sample size using the Korobov sequence, validation performance remains notably superior to the sparse quadrature baseline, but does degrade as expected (Fig. 8). The 39-member sequence performs about as well as, or better in the case of Irma, than the 59-member sequence in the lower half distribution but noticeably worse in the upper half distribution. While the 19-member sequence performs similarly to the 39-member sequence in the upper half distribution. If for practical purposes, we select the 90th percentile of the RMSE as an arbitrary measure of performance (RMSE_{90}), for all three storms the 59-member sequence has an RMSE_{90} accuracy of approximately 0.3 m. Whereas, the RMSE_{90} accuracy is approximately 0.5 m for the 39-member sequence and 0.5-0.7 m for the 19-member sequence. Therefore, in section 2 we choose the 59-member Korobov sequence as it provides about twice the accuracy of the smaller sample sizes under this assessment.

2) Water Surface Elevation Extrapolation and Logarithmic Transformation

Here we vary the number of IDW neighbors (k = [1, 4, 16]), IDW order (p = [1, 2]), and the friction factor (f_f = [0.0001, 0.0004, 0.0016]) for the water surface elevation extrapolation over dry mesh points. The friction factor values are derived through the Manning's relation, $f_f = n^2 U_f^2 / H_f^{4/3}$, with n = [0.025, 0.05, 0.1] $\mathrm{sm}^{-1/3}$ (Manning's n coefficient), H_f = 1 m (flow

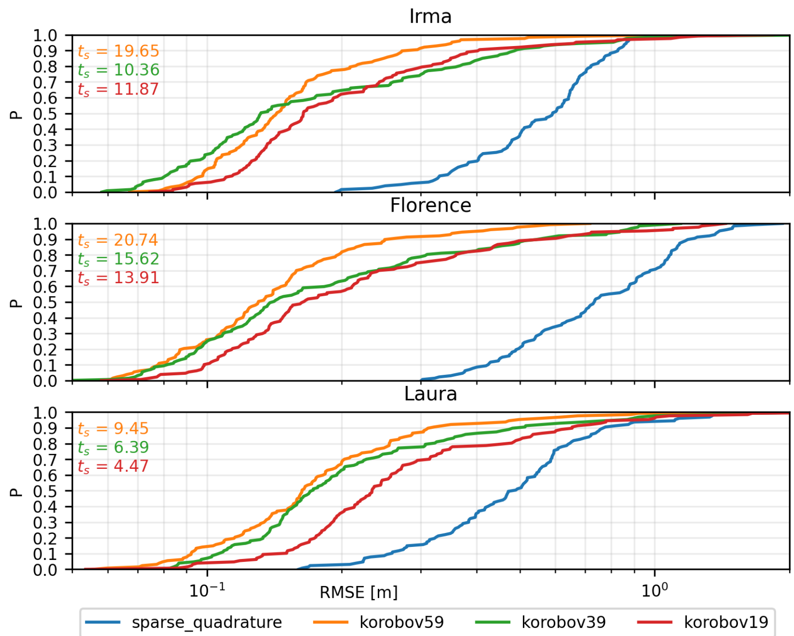

FIG. 8. CDF curves of the surrogate model RMSE across all validation members (128 samples) for the three hurricane forecasts (Irma, Florence, Laura), using 19-, 39-, and 59-member Korobov sequence training sets with ElasticNet_LOO regression. t_s is the two-sided t-test statistic between the sparse quadrature RMSE and the Korobov RMSEs corresponding to the colors in the legend (largest positive value indicates smallest average RMSE).

depth) and $U_f = 0.4$ ms^{-1} (flow velocity). The surrogate model for the $k = 1$, $p = 1$, $n = 0.05$ case is computed in log-space as well as linear-space. Results show that surrogate model accuracy is worse in terms of both RMSE and false wet/dry classification than in linear-space (Fig. 9). We also tried surrogate model generation in log-space only for mesh points that are always wet in the training set (like in section a1), which did indeed provide an improvement to the false dry classification percentage compared to linear-space (not shown). However, it would appear that when extrapolation is used over dry points and negative depths are introduced to the training set, this benefit disappears. Therefore, we only show the other extrapolation parameter experiment results in linear-space.

Surrogate model RMSE tends to increase with the friction factor, especially for $n = 0.1$ (Fig. 9). Performance for $n = 0.025$ and 0.05 are similar except for Laura, in which the smaller $n = 0.025$ is clearly superior. False wet/dry classifications follow a clear pattern where the surrogate model with

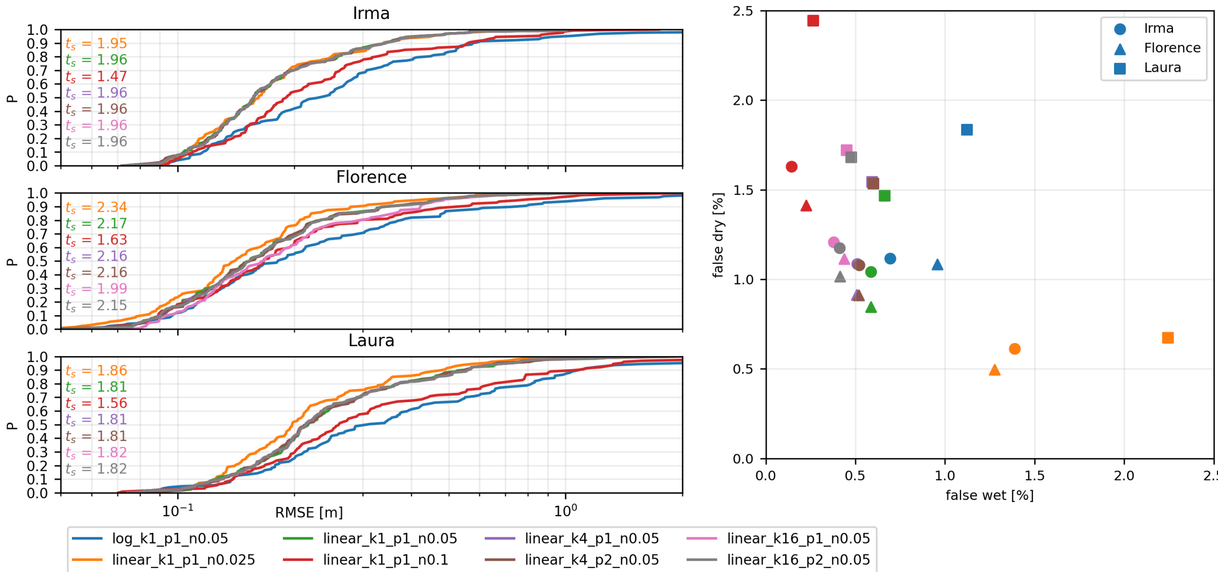

FIG. 9. Comparison of the surrogate model accuracy for different extrapolation parameters and construction in linear-space versus log-space. k and p in the legend are parameters from the extrapolation Eq. (1). n is the Manning's n coefficient used to compute f_f in Eq. (2). Results are shown across all validation members (128 samples) for the three hurricane forecasts (Irma, Florence, Laura), using 59-member Korobov sequence training sets with ElasticNet_LOO regression. Left: RMSE CDF curves, where t_s is the two-sided t-test statistic between the log-space RMSE and the linear-space RMSEs corresponding to the colors in the legend (largest positive value indicates smallest average RMSE). Right: Total percentage of mesh points across all validation members with a false wet/dry classification.

a larger friction factor gives more false dry predictions but fewer false wet predictions, and vice-versa for a smaller friction factor. In addition to the fact that the smaller friction factor produces smaller RMSEs, we prefer the smaller $n = 0.025$, since from an emergency management standpoint it would generally be considered preferable to be biased towards false wet classifications. As for the IDW extrapolation parameters, using more neighbors and going to second-order does not provide any discernible benefit to nearest neighbor ($k = p = 1$). As such, and for a preference towards simplicity, nearest neighbor using $n = 0.025$ is selected for presentation of the results in section b.

b. Probabilistic Predictions and Global Sensitivities

Maps of the sensitivities and probabilistic predictions extracted from the best surrogate model setup from section a (59-member Korobov sequence training set with ElasticNet_LOO regression and extrapolation using $n = 0.025$ ($f_f = 0.0001$) and $k = p = 1$), are shown here to demonstrate the product output. First, total effect sensitivity indices of $\boldsymbol{\lambda}$ plotted in Fig. 10 indicate that the CT error is the most sensitive variable across all storms and over most of the region. The CT sensitivity tends to be smaller on the right-hand side of the forecasted track, likely since right-hand side wind speeds are supported by the hurricane forward speed. The importance of the other error variables is somewhat storm and location dependent. V_{max} is the second-most important for Irma, while R_{max} is for Laura. Florence is approximately equally sensitive to AT, V_{max}, and R_{max}. This information could be used in conjunction with weather forecaster assessments of variable uncertainty to determine which regions have higher storm surge and inundation prediction uncertainty for the particular storm.

Second, 10%, 50%, and 90% exceedance probabilities of the maximum water surface elevations are shown in Fig. 11, illustrating how the surrogate model can predict changes to both water levels and inundation extents across the distribution. Indeed, over most of the domain the 50% exceedance probability tends to show a closer match to the best-track hindcast than the 10% or 90% probabilities. However, as expected, in the regions where a large or small maximum water surface elevation occurs in the hindcast, the match appears closer to the 10% and 90% exceedance, respectively.

More quantifiably, reliability assessments show that surrogate model probabilistic forecast has generally reasonable accuracy for all three storms (Fig. 12). The 10% exceedance for all three storms is greater than that of the best-track indicating a high-bias at this extreme end of the distribution. In comparison, at the low end (towards 90% exceedance), the Irma and Florence predictions are biased low, while Laura is consistently biased high over the whole distribution. This may be related to the higher sensitivity to R_{max} for Laura than the other storms – best-track results show a relatively localized high water surface elevation region. Notably, R_{max} is treated differently that the other error variables and is difficult to measure and forecast, motivating alternative treatment for storm size in the future.

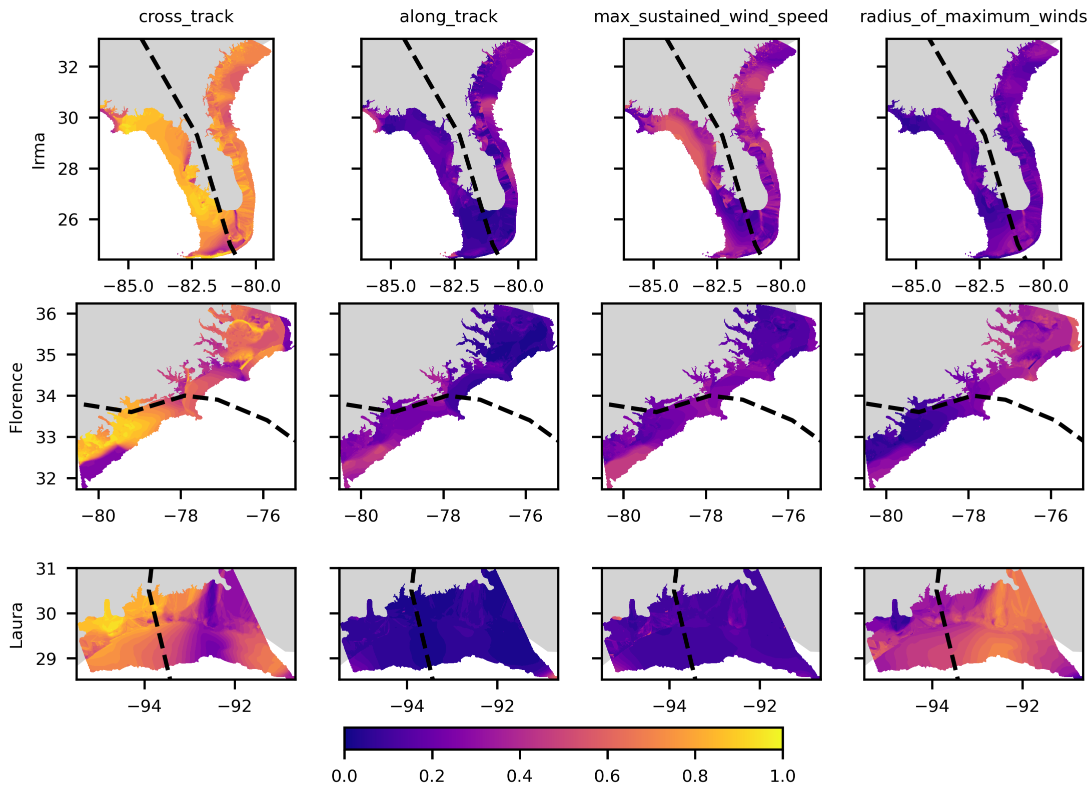

FIG. 10. Total effect sensitivity indices of maximum water surface elevation (Z) to $\boldsymbol{\lambda}$ (CT, AT, V_{max}, R_{max}) for the three hurricane forecasts (Irma, Florence, Laura). The dashed black line is the track of the NHC forecast advisory 48-hr prior to landfall. Note that mesh points with ocean depths greater than 25 m have been removed from the dataset.

Interestingly however, in terms of inundation area, the 50% exceedance probability was close to the best-track hindcast for Laura as was for Irma (Fig. 13). Though, the inundation area for Laura is more sensitive overall to the choice of exceedance probability than the other storms, highlighting the larger uncertainty for this hurricane. The inundation area for Florence is underestimated at the 50% exceedance, only matching the best-track area at the 30% exceedance. Notably, the 10% exceedance inundation area for Florence is about a factor of 2 greater than the best-track, demonstrating large uncertainty at the lower probability end of the distribution.

Comparing results for surrogate models trained on smaller sample sizes of the Korobov sequence show remarkably consistent results in terms of reliability and inundation area across all storms (Figs. 12,13). Generally, reliability of the surrogate model trained on the 19-member Korobov

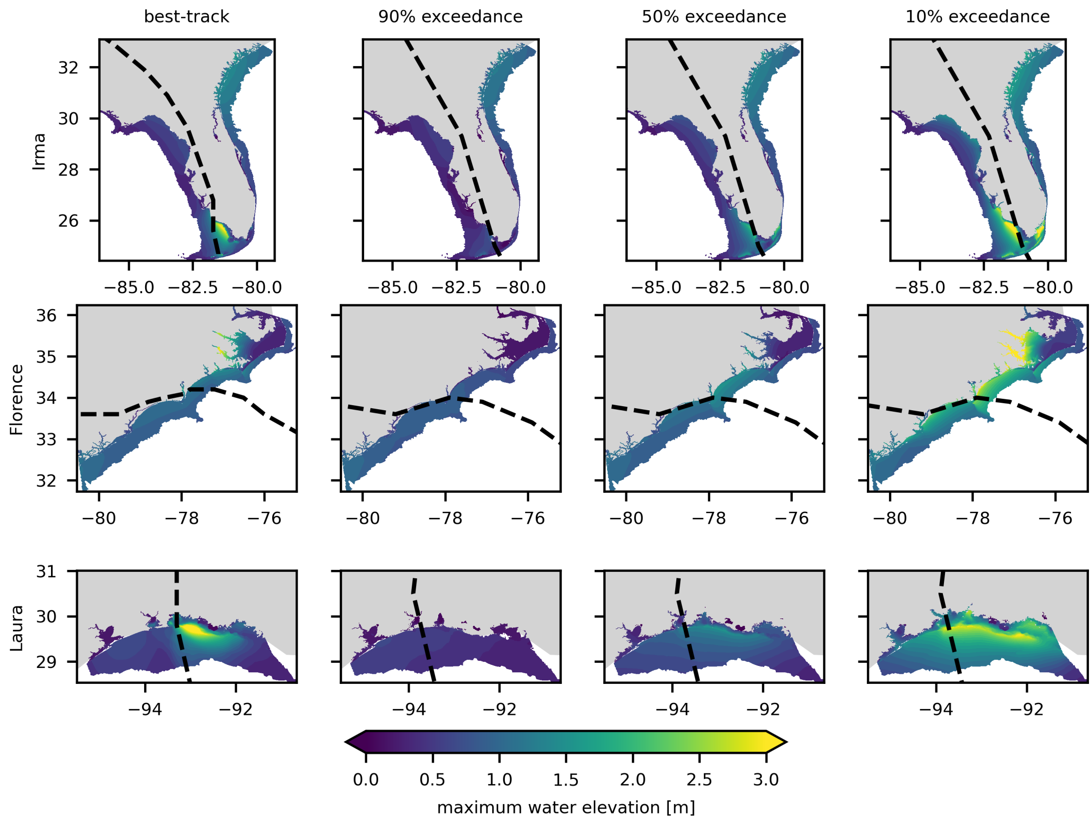

FIG. 11. Best-track hindcast and probabilistic predictions of maximum water surface elevations (10%, 50%, and 90% exceedance probabilities) for the three hurricane forecasts (Irma, Florence, Laura). The dashed black line is the best-track for the left hand side panels or the track of the NHC forecast advisory 48-hr prior to landfall in the other panels. Note that ocean depths greater than 25 m have been removed from the dataset.

sequence is at least as good as for 59 members. For Laura the reliability increases slightly as the sample sizes increase, and the best result is found from direct empirical evaluation of the 128-member validation set. For Irma and Florence, the surrogate model clearly shows improvement in reliability over direct empirical evaluation of the training and validation sets, highlighting its potential added value.

4. Discussion

The framework developed here has demonstrated that reliable probabilistic predictions of storm tide elevations and inundation can be achieved by training a KL-PC surrogate model on just $O(10)$ perturbed storm events using low-discrepancy Korobov sequences. The use of the surrogate model

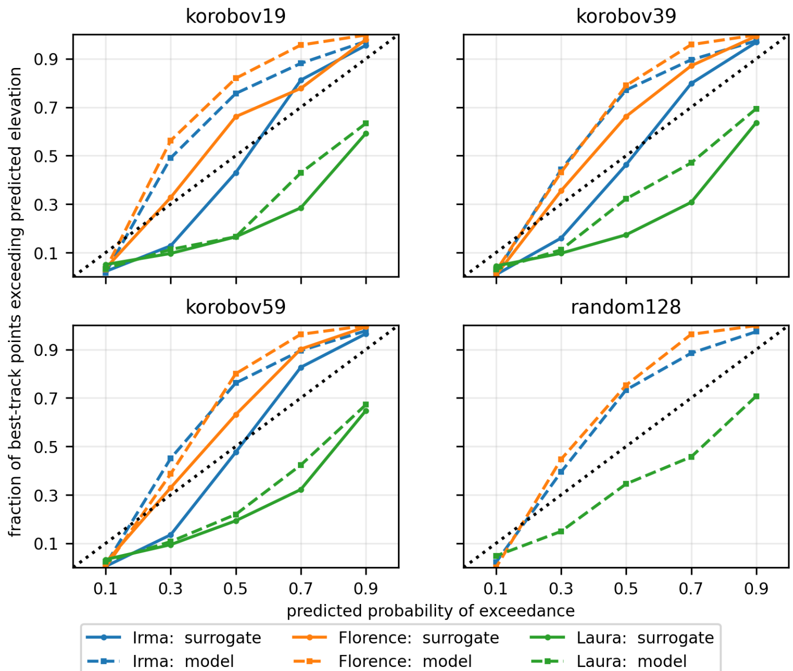

FIG. 12. Reliability plot of the 48-hr probabilistic forecast of maximum water surface elevation against the best-track hindcast for the three hurricane events (Irma, Florence, Laura). The surrogate model results are compared to direct empirical evaluation of the Korobov sequence training set used to generate the surrogate model, as well as to direct empirical evaluation of the randomly generated 128-member validation set.

was found to provide generally more reliable probabilistic predictions than the direct empirical evaluation of the training set – the added value of the surrogate model – except for Laura at moderate-high probabilities of exceedance. Moreover, the surrogate model offers additional benefits: (1) Can be used to rapidly predict the water surface elevations and inundation for any new storm perturbation; (2) Provides robust global sensitivity information, and; (3) The water surface elevation extrapolation step can be used to purposely bias surrogate inundation prediction low or high, as desired.

For determining the adequate number of training samples from the Korobov sequence, our results show that the surrogate trained on a smaller number of samples (19 here) can provide similarly reliable probabilistic predictions as the surrogate trained on more samples (39 or 59 here). Nevertheless, other results show that the surrogate from 59 samples is more accurate ($\mathrm{RMSE}_{90} \approx 1$ ft) than the surrogate from 19 samples ($\mathrm{RMSE}_{90} \approx 2$ ft) when compared to the model

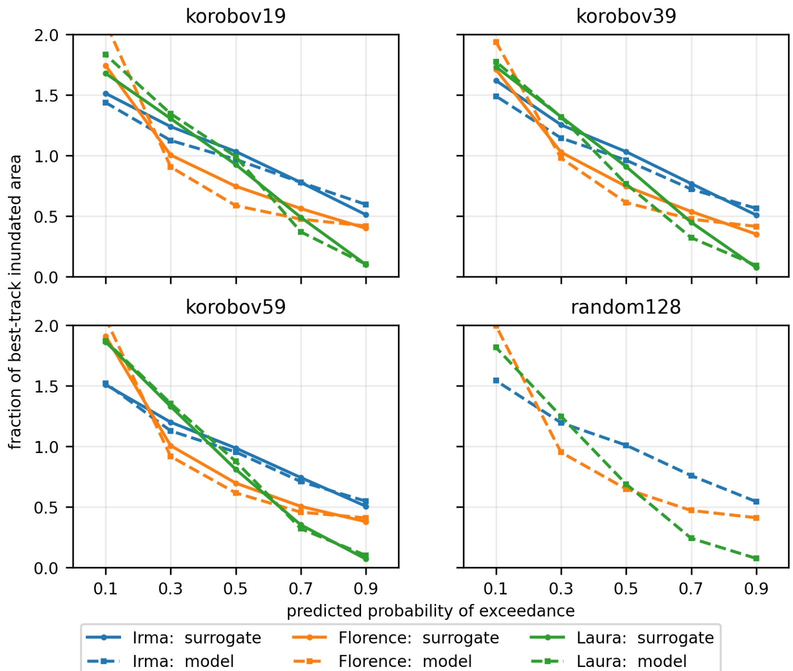

FIG. 13. Predicted inundation area of the 48-hr probabilistic forecast as a fraction of the inundation area of the best-track hindcast for the three hurricane events (Irma, Florence, Laura). The surrogate model results are compared to direct empirical evaluation of the Korobov sequence training set used to generate the surrogate model, as well as to direct empirical evaluation of the randomly generated 128-member validation set.

simulation validation set. We therefore suggest that if only the probabilistic prediction is required, and in a short time frame, that the user could select to train the surrogate using a smaller sample size (e.g., 19 which covers 90% of the distribution of λ). This is in line with previous related research that suggested 27 samples was sufficient for this purpose (Davis et al. 2010), and with Kyprioti et al. (2021a) who also demonstrates the efficiency of low-discrepancy sequences. Whereas, if the user is interested in predicting the water surface elevations for a given perturbation of the storm we recommend a higher number of training samples (e.g., 59) be used to produce a more accurate surrogate model. It is also possible that for forecasts closer to landfall, fewer training samples will be required. Note that the user is free to choose any number of samples, and is not restricted to 19, 39, and 59 used here.

In this study we used PCs due to their simplicity and usefulness in treating uncertainties. The use of penalized regression with cross-validation (we recommend Elastic Net with LOO cross-validation) was able to robustly fit the PCs across both the training and validation set, whereas OLS overfits the training set. Furthermore, it was found that the head loss water extrapolation technique for filling in dry mesh points was critical to fitting PCs accurately to overland areas. We also tried extrapolation without head loss but this resulted in poor estimation of inundation onset (generally has too many false wet predictions). Other studies without head loss extrapolation (Lee et al. 2021; Plumlee et al. 2021) used CNN and GP machine learning methods that have more degrees of freedom than PCs, which may help to hide this deficiency. Whether or not this is viewed positively or negatively, the use of PCs does lead to strong knowledge of the effect of inputs on surrogate performance. This and the fact that PCs allow for exact extraction of variance-based sensitivity indices without additional sampling highlights their usefulness for understanding uncertainty. Nevertheless, future work could explore whether ANN/CNN or GPs can improve surrogate model accuracy and reliability in our framework.

In addition to the accuracy of the surrogate model, reliability is also dependent on the hurricane perturbation methodology. In this study we followed NHC P-Surge methodology that utilizes historical statistics of forecast errors. Future work may consider how to perturb hurricane tracks in a less self-similar fashion (see Fig. 2) and with consideration of the current storm dynamics. In addition, we validated the reliability against the model simulation of the best-track hindcast, but real-world observation validation should be assessed in future. This may require the use of more sophisticated hurricane vortex models to better capture the (potentially asymmetric) wind structure and storm size. As noted, Laura was the most sensitive to R_{max} and had the lowest reliability.

Though this study focused only on the spatially varying maximum water surface elevation, the KL-PC methodology can be generally applied to a spatio-temporal surrogate construction, to account for the temporal evolution of the water surface elevations and hence predict the timing of the peak flood. Use of log-space surrogate construction to preserve surrogate model positivity when considering water level time series might be more useful than found in this study. Here, when pseudo-negative water depths were introduced into the training set from the maximum water surface elevation extrapolation, the log-space surrogate construction was found to be deleterious instead of beneficial. This is in contrast to Plumlee et al. (2021) who found the log-transform necessary for use with GPs.

5. Conclusions

A methodology for efficient ensemble perturbation of hurricane wind forcing forecasts and uncertainty quantification of the resultant simulated coastal flooding has been presented. Probabilistic prediction results based on the 48-hr forecast prior to landfall for three historical hurricanes are promising as compared to model simulations of the best-track hindcast. The methodology has been implemented into a general python framework that can be extended to develop new hurricane perturbation methodologies, use more sophisticated hurricane vortex models, and facilitate perturbations to parameters in the hydrodynamic model such as bottom roughness.

Acknowledgments. WP was supported by the U.S. National Oceanic and Atmospheric Administration (NOAA) Hurricane Supplemental grant #NA19OAR0220123 through the University Corporation for Atmospheric Research (UCAR) under a work-for-others agreement A20049 to Argonne National Laboratory through U.S. Department of Energy contract DE-AC02-06CH11357. ZB and SM were supported by the NOAA Coastal Act program through UCAR. KS was supported in part by the U.S. Department of Energy, Office of Science, Office of Advanced Scientific Computing Research, Scientific Discovery through Advanced Computing (SciDAC) Program through the FASTMath Institute. Sandia National Laboratories is a multimission laboratory managed and operated by National Technology and Engineering Solutions of Sandia, LLC., a wholly owned subsidiary of Honeywell International, Inc., for the U.S. Department of Energy's National Nuclear Security Administration under contract DE-NA0003525. We gratefully acknowledge the computing resources provided on Bebop, a high-performance computing cluster operated by the Laboratory Computing Resource Center at Argonne National Laboratory. We also would like to acknowledge support from NOAA Research and Development High Performance Computing (NOAA RDHPCS) for providing access to HERA supercomputer and Cloud resources through the ca-hsofs-c project.

Data availability statement. Data and scripts related to this manuscript are available from Pringle et al. (2022). `EnsemblePerturbation` is hosted on the NOAA Office of Coast Survey - Modeling Github website: `https://github.com/noaa-ocs-modeling/EnsemblePerturbation`, with "readthedocs" documentation linked therein.

APPENDIX

NHC Historical Forecast Error Tables

TABLE A1. Mean absolute forecast error: cross-track [nm]

	Initial V_{max} (VT=0)		
VT [hr]	< 50 kt	50-95 kt	> 95 kt
0	4.98	2.89	1.85
12	16.16	11.58	7.79
24	23.10	16.83	12.68
36	28.95	21.10	17.92
48	38.03	27.76	25.01
72	56.88	47.51	40.48
96	92.95	68.61	60.69
120	119.67	103.45	79.98

VT: forecast validation time, nm: nautical mile, kt: knot

TABLE A2. Mean absolute forecast error: along-track [nm]

	Initial V_{max} (VT=0)		
VT [hr]	< 50 kt	50-95 kt	> 95 kt
0	6.33	3.68	2.35
12	17.77	12.74	8.57
24	26.66	19.43	14.64
36	37.75	27.51	23.36
48	51.07	37.28	33.59
72	69.22	57.82	49.26
96	108.59	80.15	70.90
120	125.01	108.07	83.55

VT: forecast validation time, nm: nautical mile, kt: knot

Table A3. Mean absolute forecast error: V_{max} [kt]

	Initial V_{max} (VT=0) [kt]		
VT [hr]	< 50	50-95	> 95
0	1.45	2.26	2.80
12	4.01	5.75	7.94
24	6.17	8.54	11.53
36	8.42	9.97	13.27
48	10.46	11.28	12.66
72	14.28	13.11	13.41
96	18.26	13.46	13.46
120	19.91	12.62	13.55

VT: forecast validation time, kt: knot.

Table A4. Upper and lower bound forecast errors: R_{max} [sm]

	Initial R_{max} (VT=0) [sm]				
VT [hr]	< 15	15-25	25-35	35-45	> 45
0	[0.00,0.00]	[0.00,0.00]	[0.00,0.00]	[0.00,0.00]	[0.00,0.00]
12	[-17.15,2.47]	[-13.29.5.74]	[-11.26,10.56]	[-14.82,18.24]	[-22.40,25.43]
24	[-23.55,2.31]	[-18.16,9.45]	[-17.93,13.31]	[-12.13,21.01]	[-18.04,34.39]
36	[-24.90,4.20]	[-25.18,9.24]	[-14.88,17.36]	[-11.19,24.89]	[-1.08,43.22]
48	[-30.57,3.64]	[-29.75,9.80]	[-13.36,18.98]	[-8.47,31.64]	[8.46,43.78]
60	[-37.83,1.33]	[-27.25,10.07]	[-13.70,19.29]	[-6.35,31.09]	[8.18,43.14]
72	[-45.11,-0.99]	[-24.75,10.35]	[-14.04,19.60]	[-4.24,30.54]	[7.93,42.51]
96	[-55.26,-3.72]	[-29.71,13.94]	[-11.43,19.67]	[0.37,30.46]	[2.49,38.55]
120	[-61.26,-9.56]	[-35.46,11.77]	[-11.71,19.62]	[-0.84,32.59]	[3.19,40.56]

VT: forecast validation time, sm: US statute mile.

References

Abdolali, A., A. V. D. Westhuysen, Z. Ma, A. Mehra, A. Roland, and S. Moghimi, 2021: Evaluating the accuracy and uncertainty of atmospheric and wave model hindcasts during severe events using model ensembles. *Ocean Dynamics*, **71**, 217–235, https://doi.org/10.1007/s10236-020-01426-9.

Ayyad, M., M. R. Hajj, and R. Marsooli, 2021: Spatial Variation in Sensitivity of Hurricane Surge Characteristics to Hurricane Parameters. *Journal of Engineering Mechanics*, **147 (10)**, 04021 070, https://doi.org/10.1061/(ASCE)EM.1943-7889.0001984.

Davis, J. R., V. A. Paramygin, D. Forrest, and Y. P. Sheng, 2010: Toward the probabilistic simulation of storm surge and inundation in a limited-resource environment. *Monthly Weather Review*, **138 (7)**, 2953–2974, https://doi.org/10.1175/2010MWR3136.1.

Dietrich, J. C., and Coauthors, 2011: Modeling hurricane waves and storm surge using integrally-coupled, scalable computations. *Coastal Engineering*, **58 (1)**, 45–65, https://doi.org/10.1016/j.coastaleng.2010.08.001, URL http://linkinghub.elsevier.com/retrieve/pii/S0378383910001250.

Feinberg, J., and H. P. Langtangen, 2015: Chaospy: An open source tool for designing methods of uncertainty quantification. *Journal of Computational Science*, **11**, 46–57, https://doi.org/10.1016/j.jocs.2015.08.008.

Gonzalez, T., and A. Taylor, 2018: Development of the nws' probabilistic tropical storm surge model. *33rd Conference on Hurricanes and Tropical Meteorology*, Ponte Vedra, FL.

Hashemi, M. R., M. L. Spaulding, A. Shaw, H. Farhadi, and M. Lewis, 2016: An efficient artificial intelligence model for prediction of tropical storm surge. *Natural Hazards*, **82 (1)**, 471–491, https://doi.org/10.1007/s11069-016-2193-4.

Holland, G. J., 1980: An Analytic Model of the Wind and Pressure Profiles in Hurricanes. *Monthly Weather Review*, **108 (8)**, 1212–1218, https://doi.org/10.1175/1520-0493(1980)108<1212:AAMOTW>2.0.CO;2.

Jelesnianski, C., J. Chen, and W. Shaffer, 1992: SLOSH: Sea, lake, and overland surges from hurricanes. Tech. Rep. April, 71 pp. URL http://scholar.google.com/scholar?hl=en{\&}btnG=Search{\&}q=intitle:SLOSH:+Sea,+Lake,+and+Overland+Surges+from+Hurricanes{\#}0.

Jia, G., and A. A. Taflanidis, 2013: Kriging metamodeling for approximation of high-dimensional wave and surge responses in real-time storm/hurricane risk assessment. *Computer Methods in Applied Mechanics and Engineering*, **261-262**, 24–38, https://doi.org/10.1016/j.cma.2013.03.012, URL http://dx.doi.org/10.1016/j.cma.2013.03.012.

Jia, G., A. A. Taflanidis, N. C. Nadal-Caraballo, J. A. Melby, A. B. Kennedy, and J. M. Smith, 2016: Surrogate modeling for peak or time-dependent storm surge prediction over an extended coastal region using an existing database of synthetic storms. *Natural Hazards*, **81 (2)**, 909–938, https://doi.org/10.1007/s11069-015-2111-1.

Joyce, B., J. Gonzalez-Lopez, A. Van der Westhuysen, D. Yang, W. J. Pringle, J. J. Westerink, and A. Cox, 2019: U.S. IOOS coastal and ocean modeling testbed: Hurricane-induced winds, waves and surge for deep-ocean, reef fringed islands in the Caribbean. *Journal of Geophysical Research C: Oceans*, **124 (4)**, 2876–2907, https://doi.org/10.1029/2018JC014687, URL https://onlinelibrary.wiley.com/doi/abs/10.1029/2018JC014687.

Kim, S. W., J. A. Melby, N. C. Nadal-Caraballo, and J. Ratcliff, 2015: A time-dependent surrogate model for storm surge prediction based on an artificial neural network using high-fidelity synthetic hurricane modeling. *Natural Hazards*, **76 (1)**, 565–585, https://doi.org/10.1007/s11069-014-1508-6.

Korobov, N. M., 1959: Approximate evaluation of repeated integrals. *Dokl. Akad. Nauk SSSR*, **124**, 1207–1210.

Kyprioti, A. P., E. Adeli, A. A. Taflanidis, J. J. Westerink, and H. L. Tolman, 2021a: Probabilistic Storm Surge Estimation for Landfalling Hurricanes: Advancements in Computational Efficiency Using Quasi-Monte Carlo Techniques. *Journal of Marine Science and Engineering*, **9**, 1322, https://doi.org/10.3390/jmse9121322.

Kyprioti, A. P., A. A. Taflanidis, N. C. Nadal-Caraballo, and M. Campbell, 2021b: Storm hazard analysis over extended geospatial grids utilizing surrogate models. *Coastal Engineering*, **168**, 103 855, https://doi.org/10.1016/j.coastaleng.2021.103855, URL https://doi.org/10.1016/j.coastaleng.2021.103855.

Kyprioti, A. P., and Coauthors, 2021c: Improvements in storm surge surrogate modeling for synthetic storm parameterization, node condition classification and implementation to small size databases. *Natural Hazards*, https://doi.org/10.1007/s11069-021-04881-9, URL https://doi.org/10.1007/s11069-021-04881-9.

Lee, J.-W., J. L. Irish, M. T. Bensi, and D. C. Marcy, 2021: Rapid prediction of peak storm surge from tropical cyclone track time series using machine learning. *Coastal Engineering*, **170**, 104 024, https://doi.org/10.1016/j.coastaleng.2021.104024, URL https://doi.org/10.1016/j.coastaleng.2021.104024.

Luettich, R. A., and J. J. Westerink, 2004: Formulation and Numerical Implementation of the 2D/3D ADCIRC Finite Element Model Version 44.XX. Tech. rep., University of North Carolina at Chapel Hill & University of Notre Dame, Morehead City, NC & Notre Dame, IN, 74 pp. URL https://adcirc.org/wp-content/uploads/sites/2255/2018/11/adcirc{_}theory{_}2004{_}12{_}08.pdf.

Moghimi, S., and Coauthors, 2020: Development of an ESMF Based Flexible Coupling Application of ADCIRC and WAVEWATCH III for High Fidelity Coastal Inundation Studies. *Journal of Marine Science and Engineering*, **8**, 308, https://doi.org/10.3390/jmse8050308.

NOAA National Centers for Environmental Information (NCEI), 2022: U.s. billion-dollar weather and climate disasters. URL https://www.ncei.noaa.gov/access/billions/, https://doi.org/10.25921/stkw-7w73.

Penny, A., and J. P. Cangialosi, 2019: P-surge error update. Tech. rep., 13 pp.

Plumlee, M., T. G. Asher, W. Chang, and M. V. Bilskie, 2021: High-fidelity Hurricane Surge Forecasting using Emulation and Sequential Experiments. *Annals of Applied Statistics*, **15 (1)**, 460–480, https://doi.org/10.1214/20-AOAS1398.

Pringle, W., Z. Burnett, K. Sargsyan, S. Moghimi, and E. Myers, 2022: Efficient probabilistic prediction and uncertainty quantification of hurricane surge and inundation: Model data and analysis code. https://doi.org/10.5281/zenodo.6588627.

Pringle, W. J., D. Wirasaet, K. J. Roberts, and J. Westerink, 2021: Global Storm Tide Modeling with ADCIRC v55: Unstructured Mesh Design and Performance. *Geoscientific Model Development*, **14 (2)**, 1125–1145, https://doi.org/10.5194/gmd-14-1125-2021.

Rucker, C. A., N. Tull, J. C. Dietrich, T. E. Langan, H. Mitasova, B. O. Blanton, J. G. Fleming, and R. A. Luettich Jr., 2021: Downscaling of real-time coastal flooding predictions for decision support. *Natural Hazards*, https://doi.org/10.1007/s11069-021-04634-8.

Sargsyan, K., 2012: Adaptive basis selection and dimensionality reduction with bayesian compressive sensing. *Society for Industrial and Applied Mathematics (SIAM) Conference on Uncertainty Quantification*, Raleigh, NC.

Sargsyan, K., 2017: Surrogate Models for Uncertainty Propagation and Sensitivity Analysis. *Handbook of Uncertainty Quantification*, R. Ghanem, D. Higdon, and H. Owhadi, Eds., Springer, Cham, chap. 19, 673–698, https://doi.org/10.1007/978-3-319-11259-6_22-1.

Sargsyan, K., and Coauthors, 2021: UQTk Version 3.1.1 User Manual: SAND2021-3655. Tech. rep., Sandia National Laboratories, Livermore, California, 140 pp. https://doi.org/10.2172/1777090.

Sochala, P., C. Chen, C. Dawson, and M. Iskandarani, 2020: A polynomial chaos framework for probabilistic predictions of storm surge events. *Computational Geosciences*, **24**, 109–128, https://doi.org/10.1007/s10596-019-09898-5.

Taflanidis, A. A., A. B. Kennedy, J. J. Westerink, J. Smith, K. F. Cheung, M. Hope, and S. Tanaka, 2013: Rapid assessment of wave and surge risk during landfalling hurricanes: Probabilistic approach. *Journal of Waterway, Port, Coastal and Ocean Engineering*, **139 (3)**, 171–182, https://doi.org/10.1061/(ASCE)WW.1943-5460.0000178.

Taylor, A., and B. Glahn, 2008: Probabilistic guidance for hurricane storm surge. *Proc. 88th AMS Annual Meeting*, New Orleans, LA, 8, URL https://ams.confex.com/ams/pdfpapers/132793.pdf.

Technology Riverside Inc., and AECOM, 2015: Mesh Development, Tidal Validation, and Hindcast Skill Asessment of an ADCIRC Model for the Hurricane Storm Surge Operational Forecast System on the US Gulf-Atlantic Coast. Tech. rep., National Oceanic and Atmospheric Administration/Nation Ocean Service, Coast Survey Development Laboratory, Office of Coast Survey, 179 pp. https://doi.org/10.7921/G0MC8X6V.

Vinogradov, S. V., Y. Funakoshi, E. Myers, S. Moghimi, and J. Calzada, 2018: ADCIRC-Based Storm Surge Operational Forecast Systems at NOAA. *Annual ADCIRC User Group Meeting*, College Park, MD, USA, https://doi.org/10.17615/w9kz-kf59.